# Photoconductivity of $C_{60}$ as an Origin of Bias-Dependent Photocurrent in Organic Photovoltaics

*Won-Ik Jeong, Yang Eun Lee, Hyun-Sub Shim, Tae-Min Kim, Sei-Yong Kim, and Jang-Joo Kim**

**The bulk-ionized photoconductivity of $C_{60}$ is reported as an origin of the bias-dependent linear change of the photocurrent in copper phthalocyanine (CuPc)/$C_{60}$ planar heterojunction solar cells, based on the observation of the variation of the bias-dependent photocurrent on excitation wavelengths and the thickness-dependent photocurrent of the $C_{60}$ layer. A theoretical model, which is a combination of the Braun-Onsager model for the dissociation of excitons at the donor/acceptor interface and the Onsager model for the bulk ionization of excitons in the $C_{60}$ layer, describes the bias-dependent photocurrent in the devices very well. The bulk-ionized photoconductivity of $C_{60}$ must generally contribute to the photocurrent in organic photovoltaics, since fullerene and fullerene derivatives are widely used in these devices.**

## 1. Introduction

Bias-dependent photocurrents are an issue in organic photovoltaics (OPV) since they are related to the short-circuit current and the fill factor of the cell. Photocurrent generation in organic photovoltaics has been explained by the exciton dissociation at the donor/acceptor (D/A) interface. Since the binding energies of the excitons in organic molecules are a few tenths of an electron volt, due to their low dielectric constants and the localized electronic state, the offset of the LUMO or HOMO levels between the donor and the acceptor must be larger than the exciton binding energy in order to form geminate polaron pairs at the D/A interface. The geminate polaron pairs formed at the junctions also require the energy or electric field to be dissociated to free polarons to overcome the Coulomb attraction between the positive and negative polarons. This nature results in a dependence of the photocurrent on the applied voltage,[1–8] which cannot be explained properly by the Shockley diode model.[9] Instead, the Onsager-Braun model,[10] which describes the dissociation rate of the geminate pair at the D/A interface, has been successfully applied to describe the photocurrent–voltage relationship of bulk-heterojunction-type organic solar cells (OSCs).[1,5,7,8]

W.-I. Jeong, Y. E. Lee, H.-S. Shim, T.-M. Kim, S.-Y. Kim, Prof. J.-J. Kim
WCU Hybrid Materials Program
and Dept. Materials Science and Engineering
Seoul National University
Seoul, 151-744, Republic of Korea
E-mail: jjkim@snu.ac.kr

DOI: 10.1002/adfm.201200069

Recently, a very interesting bias-dependent photocurrent was reported in planar heterojunction (PHJ) OSCs where the photocurrent changes linearly with the applied bias, even for large negative bias as well as for small positive bias, without a detailed explanation of the mechanism.[11–13] Interestingly enough, the external quantum efficiency of the device showed that the bias dependence was observed only in the absorption region of $C_{60}$.[11] The authors attributed the origin of the phenomenon to photomultiplication[11,12] without any concrete evidence. The bias-dependent photocurrent is generally observed in PHJ OSCs adopting fullerene or fullerene derivatives as the acceptor. This behavior is also reported in poorly formed bulk heterojunction solar cells. These observations cannot be explained by the processes of charge separation at the D/A interface and charge transport in the device.

The photoactive materials, typically metal phthalocyanines and fullerenes, used in OSCs are known to have photoconductive properties. Even though several groups have reported the effects of photoconductivity of materials in PHJ OSCs,[14–16] photoconductivity has not attracted much attention so far due to its low photogeneration yield. However, the photoconductivity cannot be negligible for fullerene or fullerene derivatives, which are frequently used as acceptor materials in OSCs. Fullerene is known to possess high photoconductivity due to the formation of intermolecular charge transfer excitons.[16] Moreover, fullerene can absorb light under 500 nm, so that the photocurrent generated from this layer has the potential to comprise a significant portion of the total photocurrent. Unfortunately, there is no report, to our best knowledge, on the effect of the photoconductivity of fullerene on the photocurrent in OSCs.

In this paper, we report the photoconductivity of fullerene as an origin of the bias-dependent photocurrent in copper phthalocyanine (CuPc)/$C_{60}$-based PHJ OSCs, based on the the variation of the short circuit current density ($J_{sc}$) with the thickness of the $C_{60}$ layer, which is compared with optical modeling and the Onsager model of the photoconductivity. In addition to that, we demonstrate that the photoconductivity of $C_{60}$ contributes significantly to the total $J_{sc}$ in CuPc/$C_{60}$ solar cells and results in a linear dependence of photocurrent ($J_{ph}$) on the applied bias. To our best knowledge, this is the first report of the bulk property of the constituent materials as an origin of the photocurrent affecting the performance of OSCs. Moreover, the finding may be generally applied to most organic solar cells, since most organic solar cells use fullerene or its derivatives as the acceptor.

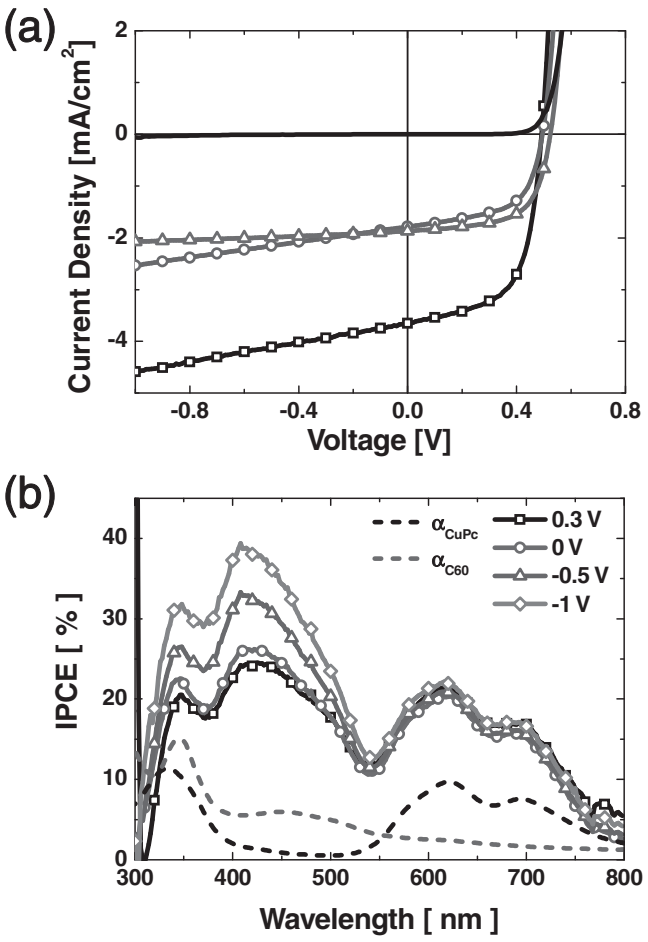


**Figure 1.** a) Current–voltage characteristics of an ITO/CuPc (20 nm)/$C_{60}$ (40 nm)/BCP (8 nm)/Al (100 nm) device under dark (solid line) and AM1.5G (black square) conditions, under the illumination of the 442 nm laser (blue circle) and 633 nm laser (red triangle). b) IPCE spectra of the device with applying bias. Dot lines represent the absorption of CuPc and $C_{60}$.

## 2. Results and Discussion

The *J–V* characteristics of the ITO/CuPc (20 nm)/$C_{60}$ (40 nm)/BCP (8 nm)/Al device are shown in **Figure 1**a. The device exhibits a power conversion efficiency (PCE) of 1.3% with a $J_{sc}$ of 4.4 mA cm$^{-2}$, an open-circuit voltage ($V_{oc}$) of 0.48 V and a fill factor (*FF*) of 0.62 under the illumination of AM1.5G solar simulated light. The performance of the device is consistent with previous reports.[17–19] It is interesting to note that the photocurrent of the device is linearly proportional to the applied voltage in the reverse-bias and in the low forward-bias regions. The variation of the photocurrent is also reflected in the incident photon-to-electron conversion efficiencies (IPCEs) of the device measured at different applied biases, as shown in Figure 1b. The IPCEs combined with the absorption spectra of the CuPc and $C_{60}$ layers clearly show that the photocurrent of this device originates from two parts: one from the CuPc donor layer due to wavelengths from 550 to 800 nm, and the other from the $C_{60}$ acceptor layer due to wavelengths from 300 to 550 nm. The contribution of each layer to the $J_{sc}$ of the device is nearly the same, with 43% (1.8 mA cm$^{-2}$) from the $C_{60}$ layer and 57% (2.37 mA cm$^{-2}$) from the CuPc layer at the short-ciruit condition. It is very interesting to note that the IPCE changes with the applied bias only in the wavelength range corresponding to the absorption of $C_{60}$, which is consistent with the previous report.[11]

Such characteristics are also manifested in the *J–V* curves of the device under the illumination of He/Cd laser (442 nm) and HeNe laser (633 nm) light, as shown in Figure 1a, to excite the $C_{60}$ and CuPc layers selectively. The laser intensities were adjusted by neutral density filters to get current densities matching those of the short-circuit condition under the solar simulated light ($J_{sc}$ of 1.79 and 1.87 mA cm$^{-2}$ by the illumination of the 442 and 633 nm laser lights, respectively). The variation of the photocurrent in the reverse bias and in the small forward bias is significant only when the $C_{60}$ layer is excited by the 442 nm laser, as expected. There is little change in the current at negative bias under the illumination of the 633 nm laser. We can conclude from the results that the bias dependence of the photocurrent originates from the charges generated from the absorption in the $C_{60}$ layer. Selective illumination of the $C_{60}$ layer in the device resulted in smaller $V_{oc}$ and *FF* results compared to the selective illumination of the CuPc layer.

The bias-dependent change of the photocurrent implies a change in the specific parallel resistance under illumination, $R_{p,light}$. Under the illumination of the solar simulator, $R_{p,light}$ is reduced to 1060 Ω cm$^2$, while the parallel resistance in the dark, $R_p$, is 35 000 Ω cm$^2$. The reduction of $R_p$ under illumination signifies the enhancement of the conductivity of the device, which has been interpreted as the increase of charge carriers due to the photovoltaic effect of the device, i.e., charge generation from the exciton dissociation at the D/A interface.[14,15,20,21] In such a case, $R_{p,light}$ can be described by

$$R_{p,light}^{-1} = R_p^{-1} + R_{p,DA'}^{-1}$$

where $R_{p,DA'}^{-1}$ represents the contribution to the device shunt from the charge generation by exciton dissociation at the D/A interface. One obvious outcome of this consideration is that the $R_{p,light}$ value must be the same under the selective illumination of the donor or acceptor layer as long as the photocurrent of the device is the same, because equal numbers of electrons and holes are generated by the dissociation of the excitons at the D/A interface no matter where the excitons are formed. In contrast to this expectation, however, the selective illumination of the CuPc and $C_{60}$ layers resulted in significantly different $R_{p,light}$ values of 4500 and 1300 Ω cm$^2$, respectively. The selective illumination of the $C_{60}$ layer gives rise to a much lower $R_{p,light}$ value than the selective illumination of the CuPc layer, implying that there is another process to produce charge-carriers in the device, which turns out to be charge generation in the bulk of the layers, especially the $C_{60}$ layer.

Evidence of the contribution of the bulk photoconductivity of the $C_{60}$ layer to the photocurrent can be obtained from the dependence of the photocurrent on the thickness of the $C_{60}$ layer. For this purpose, devices with different thicknesses of the $C_{60}$ layer were fabricated, while the thicknesses of the CuPc (20 nm) and BCP (8 nm) layers were kept constant. By adjusting the thickness of $C_{60}$ layer, the exciton distribution

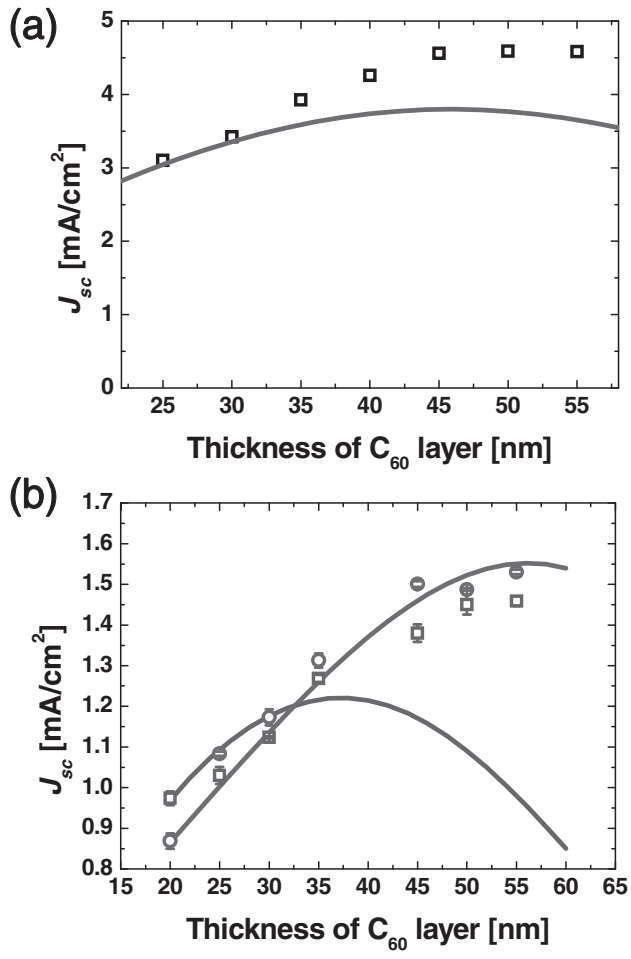


**Figure 2.** a) The change of $J_{sc}$ with varying thicknesses of the $C_{60}$ layer under AM1.5G illumination. Squares represent the experimental results and the solid line is the result of the calculation by optical simulation. b) The $J_{sc}$ values under selective excitation of the CuPc (red circle) and $C_{60}$ (blue square) layers by 633 and 442 nm laser light, respectively. Simulation results are represented by solid lines.

inside the layers could be varied. This results in a change in $J_{sc}$ due to a finite exciton diffusion length of each material if all the currents originated from the dissociation of polaron pairs at the D/A interface.

The change of $J_{sc}$ with varying $C_{60}$ thickness under the illumination of the AM1.5 solar simulated light is displayed in the **Figure 2**a, where the theoretical $J_{sc}$ values are compared with the experimental data. The theoretical $J_{sc}$ values were calculated using the transfer-matrix method under the assumption that the charges were generated only at the D/A interface. In addition, it is assumed that all excitons diffused to the D/A interface converted to charges, which were collected to the electrodes without any loss. The diffusion lengths of the excitons generated in the CuPc and $C_{60}$ layers were set to be 7 and 12 nm, respectively. The detailed procedure to calculate $J_{sc}$ can be found in the references.[18] We assumed that the change of $J_{sc}$ in Figure 2 originated mostly from the variation of the exciton distribution inside the layer, and that the effects of the imbalance of the charge-transport property[22] would not appear significantly within the thickness range within which we adjusted. This assumption is supported by the experimental data, showing only a small variation of $V_{oc}$, from 0.475 to 0.49 V, and of *FF*, from 0.61 to 0.63, between the devices with different thicknesses. The calculation results suggest that the maximum $J_{sc}$ can be obtained when the thickness of the $C_{60}$ layer is around 45 nm. However, the experimental data revealed that $J_{sc}$ increases continuously up to 55 nm. The discrepancy between the theoretical results and the experimental results gradually increased as the thickness of the $C_{60}$ layer increased.

This discrepancy can be further understood by analyzing the variation of $J_{sc}$ with the thickness of the $C_{60}$ layer under selective illumination, which is displayed in the Figure 2b. The power of the He/Cd (442 nm) and HeNe (633 nm) lasers are 19 and 22 mW cm$^{-2}$, respectively. When the CuPc layer was excited by the 633 nm laser light, the $J_{sc}$ value followed the same trends as the theoretical prediction with increasing thickness of the $C_{60}$ layer. In contrast, the selective illumination of the $C_{60}$ layer by the 442 nm laser light resulted in a significant deviation between the experimental results and the theoretical prediction. Optical calculations predicted that the $J_{sc}$ value would be maximized at a $C_{60}$ layer thickness of 35 nm, but the experimental results showed a continuous increase in the value of $J_{sc}$ up to 60 nm. Due to the finite diffusion length of the excitons, only the excitons near the interface could contribute to the charge generation. Therefore, the theoretical calculation indicates that the integrated intensity of the 442 nm laser light in the $C_{60}$ layer within the exciton diffusion length of the $C_{60}$ layer becomes a maximum when the thickness of the $C_{60}$ layer is 35 nm. Any further increase in the thickness of the $C_{60}$ layer would reduce the integrated intensity due to the interference effect of the incoming and reflected light from the cathode, resulting in a reduction of the photocurrent. The higher photocurrent obtained from the experiments compared to the theoretical prediction clearly indicates that there is another source or sources generating charges apart from the dissociation of excitons at the D/A interface. A possible source of the photocurrent generation could be bulk charge generation inside the $C_{60}$ layer. $C_{60}$ molecules are well known to have high photoconductivity and photocharge generation characteristics due to the easy formation of intermolecular charge-transfer (CT) excitons above 2.5 eV.[16,23–26]

To confirm the bulk charge generation inside the $C_{60}$ layer, a device without the donor layer (ITO/$C_{60}$(60 nm)/BCP(8 nm)/Al) was fabricated. **Figure 3** shows the *J–V* characteristics of the device under dark and AM1.5 G conditions. Under the AM1.5G condition, the device shows photovoltaic properties with a $J_{sc}$ of 0.4 mA cm$^{-2}$, a $V_{oc}$ of 0.47 V and a *FF* of 0.33, which leads to a PCE of 0.06%. In addition, the current changes linearly with an applied negative bias, which was also observed in the CuPc/$C_{60}$-based device under the selective excitation of the $C_{60}$ layer. The device shows diode characteristics in the dark (inset of Figure 3), indicating the existence of a built-in potential in the $C_{60}$ layer or a Schottky contact at the ITO/$C_{60}$ interface. An electro-absorption experiment confirmed the existence of the built-in potential in the $C_{60}$ layer indeed (not shown). Since the photocurrent was obtained without any donor/acceptor interface, we attribute the photocurrent in Figure 3 to the charge

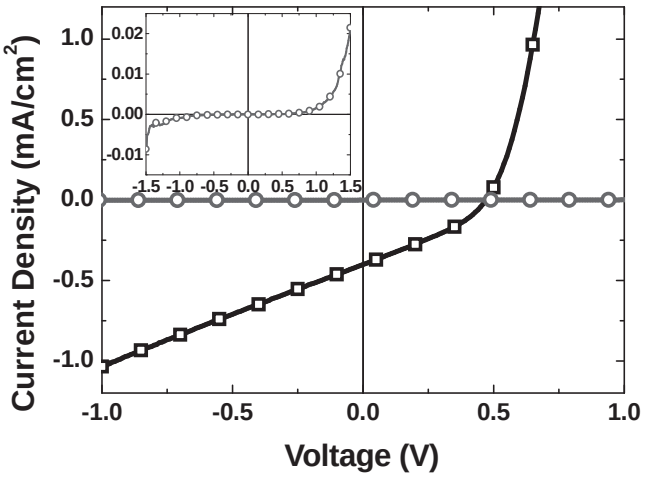


**Figure 3.** *J–V* characteristics of the ITO/$C_{60}$ (60 nm)/BCP (8 nm)/Al (100 nm) device under dark (solid line) and AM1.5G (square) conditions. The inset displays a semi-log scale of *J–V* curves with the absolute value of the current density.

generation in the bulk of the $C_{60}$ layer by the bulk ionization process. The Schottky contact or the built-in potential in the $C_{60}$ layer induces the bulk ionization and collection of electrons and holes by the internal electric field, which contributes to the photocurrent. The linear dependence of the photocurrent with the applied negative bias in Figure 3 cannot be explained if the exciton dissociation takes place at the ITO/$C_{60}$ junction because the exciton diffusion length is not influenced by the applied bias. Zhang et al. have also reported the photocurrent from an organic Schottky junction device with the structure ITO/$MoO_3$/$C_{60}$/Bphene/Al.[13,27]

Based on this observation, we can now calculate the photocurrent including the charge generation by the dissociation of geminate electron–hole pairs formed at the D/A interface by the diffusion of excitons and the charge generation in the bulk of the $C_{60}$ layer by photoionization. The dissociation current at the D/A interface can be formulated by the Braun-Onsager model,[1,7,10] where the current density can be evaluated by the combination of the exciton flux to the interface and the dissociation yield, $P(F_I,T)$, as

$$J_{ph,interface}(V) = q\,D\left.\frac{dn(x)}{dx}\right|_{x=interface} P\,(F_I,\,T) \quad (1)$$

where $q$ and $D$ are the unit charge and the diffusivity of excitons, respectively. The symbol $n(x)$ represents the exciton density as a function of position. The exciton flux can be obtained from optical modeling. $P(F_I,T)$ is calculated using the dissociation rate, $k_d$, and the recombination rate of polaron pairs, $k_f$, as

$$P(F_I,\,T) = k_d/(k_f + k_d)$$

where $k_d$ is a function of the interfacial electric field. $F_I$, and $k_d$ were calculated following the literature.[7,16,28] The model has been successfully applied to describe the behavior of $J_{ph}$ in OSCs and in a bulk heterojunction solar cell.[7,28]

The charge generation induced from the photoconductivity has been widely investigated so far. Most of the models are based on the Onsager theory of geminate recombination and use its analytic form to interpret the field-dependent bulk ionization.[16,29] In the case of OSCs, usually a low-level electric field, lower than $10^5$ V cm$^{-1}$, is applied to characterize the device performance. At a low level of the electric field, the bulk-ionization yield can be described by a simple expression as follows:

$$\Phi(F) = \left[1 + \frac{r_c}{2kT}F\right]\exp(-r_c/r_0) \quad (2)$$

where $k$ is the Boltzman constant and $F$ is the applied electric field. The symbol $r_c$ stands for the Coulumbic capture radius, with $r_c = q^2/4\pi\varepsilon_r\varepsilon_0 kT$, and $r_0$ is the thermalization distance. The photocurrent generated by bulk ionization can then be represented as $J_{ph} = qG\Phi(F)$ with the exciton generation rate, $G$. Equation 2 reveals the linear dependence of the photocurrent yield on the applied bias. Then, the photocurrent of the device can be expressed with a combination of Equation 1 and 2, as

$$J_{ph}(V) = q\,D\left.\frac{dn(x)}{dx}\right|_{x=interface} P(F,\,T) + q\frac{\Phi(F,\,T)}{\tau}\int_0^d n(x)\,dx \quad (3)$$

The second term in Equation 3 representing the current generation from the bulk ionization reveals that the linear dependence of $J_{ph}$ mainly originates from the bulk charge generation, because the $J_{ph}$ coming from the first term will be saturated under a sufficiently large negative bias. In our case, the photoconductivity of CuPc is expected to be negligible so that only the first term of Equation 3 will be of significance when exciting the CuPc layer. On the other hand, the excitons formed in the $C_{60}$ layer can produce charges by both the exciton dissociations at the D/A interface and also those originating from the bulk ionization. From that, the integration of the second term of Equation 3 would be the exciton density distributed only in the $C_{60}$ layer. In addition, the electric field, $F$, should be the localized electric field in the $C_{60}$ layer. Without consideration of the band bending, the $F$ value in the $C_{60}$ layer was simply given by $F = (V_{bi,C60} - V)/d$, where $V_{bi,C60}$ is the built-in voltage in the $C_{60}$ layer and $d$ is the thickness of the $C_{60}$ layer. The exciton density in the $C_{60}$ layer was obtained from optical calculations.

**Figure 4**a shows the calculated $J_{ph}$–$V$ characteristics originating from the dissociation of excitons at the D/A interface, the bulk ionization in the $C_{60}$ layer, and the summation of both processes; these are compared with the experimental data. $J_{ph}$ is obtained by subtracting the dark current from the current under illumination. The parameters used to fit the $J_{ph}$–$V$ curves are summarized in **Table 1**. The combined model fits the experimental result very well. It is observed that the contribution of the photoconductivity to the device photocurrent cannot be neglible. At the short-circuit condition, the photocurrent from the $C_{60}$ layer bulk is about 0.7 mA cm$^{-2}$ while the total $J_{sc}$ of the device is 4.36 mA cm$^{-2}$. One can notice that the $J_{ph}$ generated by the interface dissociation already saturates at the short-circuit condition. This behavior confirms that the linear change of $J_{ph}$ in relation to the applied bias mainly originates from the charge generation by the bulk ionization processes in the $C_{60}$ layer, which also results in the spectral change of the IPCE with

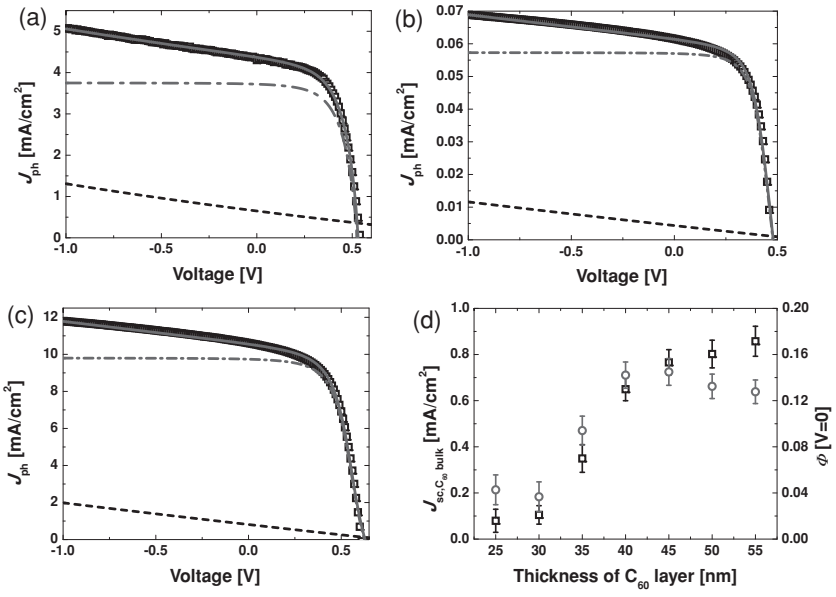


**Figure 4.** $J_{ph}$–$V$ curves of the ITO/CuPc (20 nm)/$C_{60}$ (40 nm)/BCP (8 nm)/Al (100 nm) device under the illumination of: a) AM 1.5G solar simulated light, and, b,c) 442 nm laser light with the intensities of 5 and 380 mW cm$^{-2}$, respectively. Experimental results are represented by squares. The calculated $J_{ph}$ values are from bulk ionization in the $C_{60}$ layer (dashed line), dissociation at the D/A interface (dashed dot line), and our model (solid line). d) The variation of the photocurrent generated by bulk ionization in the $C_{60}$ layer at 0 bias (square) and the bulk ionization yield (circle) with the thickness of the $C_{60}$ layer under the illumination of AM 1.5G solar simulated light.

the applied bias, shown in Figure 1. For concrete support of the suggested model, the photocurrents measured at different intensities of 442 nm laser light are displayed in Figure 4b and c. The same parameters, in Table 1, were used for the model fitting. The matching between the model and the experimental data are again excellent.

Figure 4d displays the thickness dependence of the bulk charge generation in the $C_{60}$ layer. The current from the bulk of the $C_{60}$ layer gradually increases as the thickness of the $C_{60}$ layer increases. Even though the integrated number of excitons within the diffusion length from the D/A interface in the $C_{60}$ layer shows a maximum at around 35 nm, the total number of excitons generated in the $C_{60}$ layer increases continuously as the thickness of the $C_{60}$ layer increases, leading to an enhanced contribution of the bulk charge generation to the photocurrent with increasing thickness of the $C_{60}$ layer. The bulk-ionization yield was calculated from the bulk-ionization current divided by the total number of excitons generated within the $C_{60}$ layer. It is around 4% for a 30 nm thickness of $C_{60}$ layer. However, it reaches about 14% when the $C_{60}$ layer is thicker than 40 nm.

**Table 1.** Parameters used in the $J_{ph}$ calculations.

| Parameter | Value |
|---|---|
| Polaron pair recombination rate, $k_f$ | $5.0 \times 10^5$ s$^{-1}$ |
| Exciton lifetime, $\tau(0)$ | 0.7 ns |
| $<\mu>$ | 0.001 V cm$^{-1}$ |
| Polaron pair separation distance | 1.6 nm[28] |
| $V_{bi}$ | 0.45 V |
| Thermalization distance, $r_0$ | 3.0–3.1 nm |
| $<\varepsilon>$ | 3.4[28] |
| $\varepsilon$ of C60 | 4.5[16] |

## 3. Conclusions

We have demonstrated that the linear dependence of the photocurrent in CuPc/$C_{60}$-based PHJ OPVs under reverse-bias and small forward-bias conditions originates from the bulk-ionized photoconductivity of $C_{60}$. This argument is supported by the different behavior of the bias dependence of the photocurrent and the different dependence of the photoconductivity on the thicknesses of the CuPc and $C_{60}$ layers when the CuPc or the $C_{60}$ layer was selectively excited. The bulk-ionized photocurrent in the $C_{60}$ layer contributes a significant portion of the total photocurrent generated in the OPVs. A theoretical model was successfully developed to describe the photocurrent–voltage characteristics of the device by including not only the charge generation from the exciton dissociation at the D/A interface, but also the photo-ionization of the excitons in the $C_{60}$ layer coming from the easy formation of intermolecular CT excitons in $C_{60}$. The bulk-ionized photoconductivity of $C_{60}$ must generally contribute to the photocurrent in organic photovoltaics, since fullerene and fullerene derivatives are widely used in such devices.

## 4. Experimental Section

The devices have the structure ITO/copper phthalocyanine (CuPc)/$C_{60}$/bathocuproine (BCP)/Al. CuPc and BCP were purchased from Lumtec, and $C_{60}$ from SES Research. All the layers of the OPV devices were successively deposited on UV–$O_3$-treated ITO glass substrate by thermal evaporation under high vacuum conditions (around $10^{-7}$ torr) without breaking the vacuum, followed by encapsulation with a glass can in an $N_2$ environment before the test. The thickness of the CuPc and $C_{60}$ layers were varied systematically, while the thickness of the BCP layer was kept constant at 8 nm. The Al cathode had a thickness of 100 nm. The active area of each device was 0.04 cm$^2$.

The photovoltaic properties of the devices were measured under the illumination of a solar simulator (Oriel, 69911; Newport, Stratford, CT, USA) calibrated to the AM1.5G condition with a National Renewable Energy Laboratory-certified reference Si-solar cell covered with a KG-5 filter. A He/Cd laser (442 nm) and a HeNe laser (633 nm) were also used as excitation sources; these lasers selectively excite the CuPc and $C_{60}$ layers, respectively. The intensities of the laser light sources were modulated by neutral density filters. Spectral response and IPCE were measured with a 1000 W Xe lamp (Oriel) combined with a calibrated monochromator (Acton research, SP150). The intensity of the monochromatic light was calibrated with a Si-photodiode (Newport).

The $J_{sc}$ obtained by the integration of the IPCE spectrum agreed with the measured value from the illumination of the solar simulator to within a few percent. The dark current was subtracted from the photocurrent when measuring the IPCE under applied bias.

## Acknowledgements

This work was supported by Korea's New & Renewable Energy R&D program (20093020010040) under the Ministry of Knowledge Economy, by a Korea Research Foundation NCRC grant (R15-2008-006-01001-1) and by the WCU (World Class University) project through the National Research Foundation of Korea funded by the Ministry of Education, Science and Technology (R31-2008-000-10075-0).

Received: January 10, 2012
Revised: February 24, 2012
Published online: April 17, 2012

[1] T. M. Clarke, J. R. Durrant, *Chem. Rev.* **2010**, *110*, 6736.
[2] R. A. Street, M. Schoendorf, A. Roy, J. H. Lee, *Phys. Rev.B.* **2010**, *81*, 205307.
[3] R. A. Marsh, J. M. Hodgkiss, R. H. Friend, *Adv. Mater.* **2010**, *22*, 3672.
[4] W.-I. Jeong, J. Lee, S.-Y. Park, J.-W. Kang, J.-J. Kim, *Adv. Funct. Mater.* **2011**, *21*, 343.
[5] M. Lenes, M. Morana, C. J. Brabec, P. W. M. Blom, *Adv. Funct. Mater.* **2009**, *19*, 1106.
[6] R. A. Street, S. Cowan, A. J. Heeger, *Phys. Rev. B.* **2010**, *82*, 121301(R).
[7] V. D. Mihailetchi, L. J. A. Koster, J. C. Hummelen, P. W. M. Blom, *Phys. Rev. Lett.* **2004**, *93*, 216601.
[8] M. Limpinsel, A. Wagenpfahl, M. Mingebach, C. Deibel, V. Dyakonov, *Phys. Rev. B* **2010**, *81*, 085203.
[9] A. L. Fahernbruch, R. H. Bube, *Fundamentals of Solar Cells*, Academic Press, New York **1983**.
[10] C. L. Braun, *J. Chem. Phys.* **1984**, *80*, 4157.
[11] J. Huang, Y. Yang, *Appl. Phys. Lett.* **2007**, *91*, 203505.
[12] J. Reynaert, V. I. Arkhipov, P. Heremans, J. Poortmans, *Adv. Funct. Mater.* **2006**, *16*, 784.
[13] M. Zhang, H. Wang, C. W. Tang, *Appl. Phys. Lett.* **2010**, *97*, 143504.
[14] B. P. Rand, D. P. Burk, S. R. Forrest, *Phys. Rev. B* **2007**, *75*, 115327.
[15] C. Waldauf, M. C. Scharber, P. Schilinsky, J. A. Hauch, C. J. Brabec, *J. Appl. Phys.* **2006**, *99*, 104503.
[16] M. Pope, C. E. Swenberg, in *Electronc Processes in Organic Crystals and Polymers*, 2nd ed., Oxford University Press, New York **1999**.
[17] I. Hancox, P. Sullivan, K. V. Chauhan, N. Beaumont, L. A. Rochford, R. A. Hatton, T. S. Jones, *Org. Electron.* **2011**, *11*, 2019.
[18] J. Lee, S. Y. Kim, C. S. Kim, J.-J. Kim, *Appl. Phys. Lett.* **2010**, *97*, 083306.
[19] J. W. Kim, H. J. Kim, H. H. Lee, T. Kim, J.-J. Kim, *Adv. Funct. Mater.* **2011**, *21*, 2067.
[20] J. R. Tumbleston, D.-H. Ko, E. T. Samulski, R. Lopez, *J. Appl. Phys.* **2010**, *108*, 084514.
[21] S. Yoo, B. Domercq, B. Kippelen, *J. Appl. Phys.* **2005**, *97*, 103706.
[22] W. Tress, A. Petrich, M. Hummert, M. Hein, K. Leo, M. Riede, *Appl. Phys. Lett.* **2011**, *98*, 063301.
[23] J. Mort, M. Machonkin, R. Ziolo, I. Chen, *Appl. Phys. Lett.* **1992**, *61*, 1829.
[24] R. Konenkamp, R. Engelhardt, R. Henninger, *Solid State Commun.* **1995**, *97*, 285.
[25] D. Dick, X. Wei, S. Jeglinski, R. E. Benner, Z. V. Vardeny, D. Moses, V. I. Srdanov, F. Wudl, *Phys. Rev. Lett.* **1994**, *73*, 2760.
[26] S. Kazaoui, R. Ross, N. Minami, *Phys. Rev. B* **1995**, *52*, R11665.
[27] M. Zhang, Irfan, H. Ding, Y. Gao, C. W. Tang, *Appl. Phys. Lett.* **2010**, *96*, 183301.
[28] N. C. Giebink, G. P. Wiederrecht, M. R. Wasielewski, S. R. Forrest, *Phys. Rev. B* **2010**, *82*, 155305.
[29] L. Onsager, *Phys. Rev.* **1938**, *54*, 554.